^{33}Cl Spectroscopic Factors via the ^{32}S(^{3}He, d)^{33}Cl One-Proton Transfer Reaction

M Cinausero[1], D Dell'Aquila[2,3], I Lombardo[4], M Vigilante[5,4], S Barlini[7], R Bolzonella[11,1], M Bruno[8,9], A Buccola[10,7], S Cartuan[1], G Casini[7], M Cicerchia[12,1], M D'Andrea[4], M Degerlier[14], D Fabris[11], L Gasques[13], F Gramegna[1], A Lepine-Szily[13], G Mantovani[12,1], T Marchi[1], S Piantelli[7], V Rigato[1], L Scomparin[12,1] and S Valdrè[7]

[1] INFN-Laboratori Nazionali di Legnaro, Legnaro, Italy
[2] Dipartimento di Scienze Chimiche, Fisiche, Matematiche e Naturali, University of Sassari, Sassari, Italy
[3] INFN-Laboratori Nazionali del Sud, Catania, Italy
[4] INFN-Sezione di Catania, Catania, Italy
[5] Università degli Studi di Napoli "Federico II", Napoli, Italy
[6] INFN-Sezione di Napoli, Napoli, Italy
[7] INFN-Sezione di Firenze, Firenze, Italy
[8] Università degli Studi di Bologna, Bologna, Italy
[9] INFN-Sezione di Bologna, Bologna, Italy
[10] Università degli Studi di Firenze, Firenze, Italy
[11] INFN-Sezione di Padova, Padova, Italy
[12] Università degli Studi di Padova, Padova, Italy
[13] Instituto de Fisica da Universidade de São Paulo, 05508-090 São Paulo, Brasil
[14] Science and Art Faculty, Physics Department, Nevsehir Haci Bektas Veli Univ., Nevsehir, Turkey

E-mail: ddellaquila@uniss.it

Abstract. The structure of light-to-medium mass nuclei is crucial to understand exotic phenomena in nuclear structure, including the appearance of molecular effects in light nuclei and their impact in nuclear astrophysics. In this paper, a new experiment to probe one-proton spectroscopic factors of bound and unbound states in the *sd*-nucleus ^{33}Cl is discussed. The experiment exploits the reaction ^{32}S(^{3}He, d)^{33}Cl* at 9.68 MeV bombarding energy. This reaction is suitable to probe the single-particle structure of ^{33}Cl states with respect to the population of $1d_{3/2}$, $1f_{7/2}$ and $2p_{3/2}$ shells. Crucial aspects of the investigation are the use of an enriched, high-purity, ^{32}S target and a new generation hodoscope with improved angular resolution, allowing to obtain high-precision angular distribution of the differential cross section in a broad angular range. Results are interpreted by means of finite-range DWBA and coupled-channel calculations.

1. Introduction

The investigation of nuclear reactions at low and intermediate energies has a paramount importance to understand the atomic nucleus. It allows to investigate the detailed properties of the structure of nuclear systems [1, 2, 3], the occurrence of continuum effects [4, 5, 6], the appearance of exotic configurations [7], clustering phenomena [8, 9, 10, 11], and their influence

in astrophysics [12, 13, 14]. Another important aspect observed in nucleus-nucleus collisions concerns their dynamical evolution [15, 16, 17, 18], and the interplay between structure and dynamics [19, 20]. The latter usually requires the investigation of heavy-ion collisions at moderately high energies and the use of 4π detectors [21, 22], as the corresponding final states contain a large number of charged particles, gamma-rays, and neutrons [23]. On the other hand, nuclear spectroscopy studies are typically more selective, enabling the use of more compact and often modular devices [24, 25, 26] (which are also used as ancillary systems for large acceptance detectors at higher energies, see e.g. Refs. [27, 28, 29, 30, 31, 32]).

In this framework, transfer reactions are a class of particularly selective processes that allow to explore specific degrees of freedom in nuclear systems such as single-particle configurations. Recently, a number of transfer reaction channels have been investigated using high-precision spectrometers such as MAGNEX at INFN-LNS [33], VAMOS at GANIL [34] and K600 at iThemba LABS [35]. To contribute in the field, we have developed a new high-resolution and modular detector, OSCAR, capable to identify light charged particles with high angular resolution and low detection thresholds [36]. The newly developed detector has the advantage of high angular segmentation, high energy resolution and a high degree of modularity, and is thus ideal to investigate transfer reactions at low and intermediate energies.

In this paper, we exploit the new modular device OSCAR to investigate the one-proton transfer reaction ^{32}S(^{3}He,d)^{33}Cl at 9.68 MeV incident energy. This reaction allows to probe the spectroscopy (i.e. energy, J^{π}, and $C^{2}S_{p}$ spectroscopic factors) of low-lying states in the the *sd*-shell ^{33}Cl nucleus. When a transfer reaction channel is investigated experimentally, the goal is to measure differential cross section angular distributions in absolute units, for several excited states of the residual nucleus. To obtain information on the spectroscopy of the residual nucleus, one has to compare them with the predictions of theoretical calculations [37, 38]. In this way, one can estimate one-proton spectroscopic factors $C^{2}S_{p}$ for various excited states in ^{33}Cl, allowing to benchmark modern shell model approaches. For example, in Ref. [37], the authors used different surface interactions to perform shell model calculations on *sd*-shell nuclei, including ^{33}Cl. Energy positions and spectroscopic amplitudes for low energy states in this nucleus have been calculated with MSDI and FPSDI interactions [37]. In addition, alternative approaches, such as the Intermediate-Coupling Vibrational Model (ICV) [38], had a discrete success in reproducing the spectroscopy of ^{33}Cl.

However, while the theory reached a level of good consistency, from the experimental point of view several ambiguities are still affecting the spectroscopy of ^{33}Cl at low excitation energies. These ambiguities concern in particular J^{π} assignments and $C^{2}S_{p}$ spectroscopic factors [39]. To improve previous studies of the ^{32}S(^{3}He,d)^{33}Cl reactions [40, 41], an essential ingredient is to reduce possible sources of contaminants produced by undesired elements in the target and, additionally, to improve energy and angular resolution to more effectively disentangle the background from the signals to measure. In our experiment, we devote large care to the choice of the experimental target, and the identification of contaminant reactions. In addition, the absolute units of the measured differential cross section are obtained via an internal normalization procedure.

Finally, these studies have also an astrophysical relevance. The ^{32}S(^{3}He,d)^{33}Cl reaction is a valid surrogate method to indirectly constrain the ^{32}S(p,γ)^{33}Cl reaction rate at the astrophysical temperatures, which is particularly difficult to analyze with direct methods due to the Coulomb barrier. To this end, $C^{2}S_{p}$ values determined from transfer reactions can be used to evaluate the resonance strength [42].

2. Experimental setup

The experiment exploited a high-quality ^{3}He^{++} beam accelerated by the CN accelerator of the INFN-Laboratori Nazionali di Legnaro (LNL), Italy, at an energy of 9.68 MeV. We used

a $^{nat}Zn^{32}S$ target with a thickness of 53 $\mu g/cm^2$. To reduce contaminant reactions, possibly arising from other elements present in the target, the sulfur used to produce the target was 99% enriched in ^{32}S. In addition, the $^{nat}Zn^{32}S$ powder was evaporated by electron beam technique on a thin substrate of carbon ($\approx$ 15 $\mu g/cm^2$). Detectors were installed on a rotating plate, which hosted the OSCAR telescope in its nominal configuration (see Ref. [36] for further details), and 2 additional telescopes, each constituted by an ORTEC surface barrier silicon followed by a high resolution Hamamatsu PIN diode. The latter were used for monitoring purposes, while OSCAR was used to measure the reaction differential cross section of the process of interest.

The OSCAR telescope is constituted by an ultra-thin ($\approx$ 20 μm) 16-strips Single-Sided Silicon Strip Detector (SSSSD), manufactured by Micron Semiconductors, used as the first detection stage, and 16 silicon PIN photodiodes (300 μm thick), manufactured by Hamamatsu, used as the second detection stage. The strips in the first detection stage have a pitch of 3.125 mm and are arranged vertically. The silicon pads in the second detection stage have a square surface with an active area of 1 cm^2 and a ceramic frame of 1.4 mm at all sides except the bottom one, where a frame of 3.2 mm is present. Each pad is installed on an electronic board containing plug-in pre-amplifiers, while for the first detection stage we used a dedicated 16 channels pre-amplifier which lies below the rotating plate.

The angular position of each detector with respect to the beamline and the target was carefully measured using an optical alignment system. We obtained an overall accuracy on the positioning better than about 0.2°. The optical alignment procedure allowed us also to benchmark the geometry information of the SSSSD detector claimed by the manufacturer. The OSCAR hodoscope allows, in turn, to obtain 64 individual detection units, by exploiting the correlations between the first and second detection stages. This allows to precisely constrain the impact point on the surface of the detector and therefore the emission angle of the particle emitted from the target. We call these detection units pseudo-telescopes, being each of those identified by the correspondence of a particular strip of the SSSSD with a pad in the second detection stage. For simplicity, the detection angle associated with each pseudo-telescope is defined as the geometrical center of the corresponding strip-pad correspondence. The latter are estimated using a dedicated Monte Carlo simulation of the setup. Optical measurement data are used to constrain the simulations. Effective solid angles of each pseudo-telescope were benchmarked by means of a dedicated Monte Carlo tool as described in Ref. [36]. In the present experiment, OSCAR was used in two different angular configurations, obtained by suitably rotating the plate hosting the detectors. The geometrical solid angle covered by OSCAR in the two configurations had a small overlap, which allowed us to further test the consistency of our data. In this way, OSCAR covered a larger region of detection angles than state-of-the-art experiments previously published in the literature [40, 41]. In the first of the two geometry positions, OSCAR covered the laboratory angles from about $\theta = 20°$ to about $\theta = 40°$, while in the second the laboratory angles from $\theta = 40°$ to $\theta = 60°$ are covered.

3. Data Anaysis and Interpretation

OSCAR allows to highly accurately reconstruct charged particles by correlating strips in the first detection stage with pads in the second detection stage. This is obtained with a dedicated geometrical coherence algorithm, as described in Ref. [36]. The energy deposited in the detector was calibrated independently for the first and the second stage by using the elastic scattering $^3He + ^{197}Au$ at 13 different incident energies, collected at the end of the experimental run. This gave the possibility to obtain highly reliable calibrations for all strips and pads in the array. To account for small electronic drift effects, which have an impact on the quality of the energy calibration while merging data collected at different times during the experiment, we have produced a correction factor for each pseudo-telescope and each individual run of the experiment. Data from all runs were then merged, maximizing the statistics.

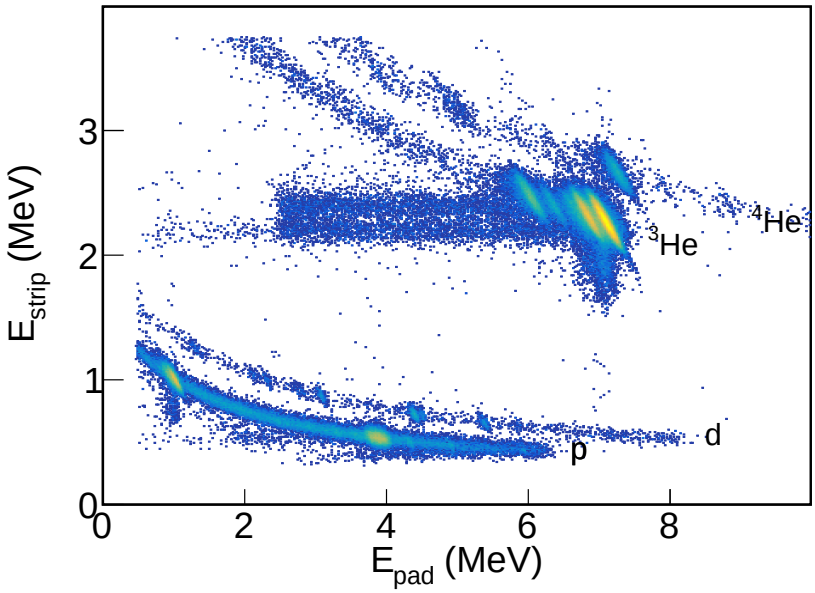

Figure 1. An example of ΔE-E scatter plot, measured with one pseudo-telescope of the OSCAR device, used to identify deuterons. Both axes are calibrated in MeV. Bumps observed on the deuteron line are produced by (^{3}He,d) on ^{32}S and the contaminants ^{12}C and ^{16}O.

Light charged particles were identified using the ΔE-E identification technique, exploiting calibrated energies in the first (E_{strip}) and second (E_{pad}) detection stages of OSCAR. The underlying procedure was repeated, individually, for each pseudo-telescope, allowing to minimize the loss of resolution due to thickness variation of the first stage. Figure 1 shows a typical ΔE-E plot obtained using data from a pseudo-telescope. Protons, deuterons, ^{3}He and ^{4}He are clearly identified. Bumps lying on the observed ΔE-E loci are produced mainly by the occurrence of binary nuclear processes, such as scattering or binary reactions. The deuteron locus exhibits interesting structures, with a low background level, due to deuterons emitted from (^{3}He,d) two-body reactions. These reactions include the one-proton transfer reactions investigated in the present analysis.

Data analysis takes into consideration deuteron and ^{3}He loci. The first is used to estimate the yield of all (^{3}He,d) reactions on ^{32}S, while, the second is used for the internal normalization of the differential cross section. In order to properly disentangle various (^{3}He,d) reactions induced on our target, we studied the kinematic lines associated to well-reconstructed deuterons in OSCAR. This represents a crucial advantage, with respect to investigations involving smaller acceptance detectors. In the present case, thanks to the use of a hodoscope of highly segmented detectors, numerous detection units are available in a unique geometrical configuration of the setup. Figure 2 shows kinematic lines E_{kin} vs θ_{lab} obtained for well-reconstructed deuterons in both geometrical configurations used in the experiment. OSCAR covered the polar angular region $20^\circ \leq \theta \leq 60^\circ$ in the laboratory frame. We can clearly identify a number of lines, which reflect the corresponding processes. The experimental lines are compared to kinematical calculations, which accounted also for the loss of energy in the target before the deuterons are detected. We indicate with the red dashed lines the calculations assuming that deuterons are emitted from the ^{32}S(^{3}He,d)^{33}Cl reactions, for different excitation energy states of the residual

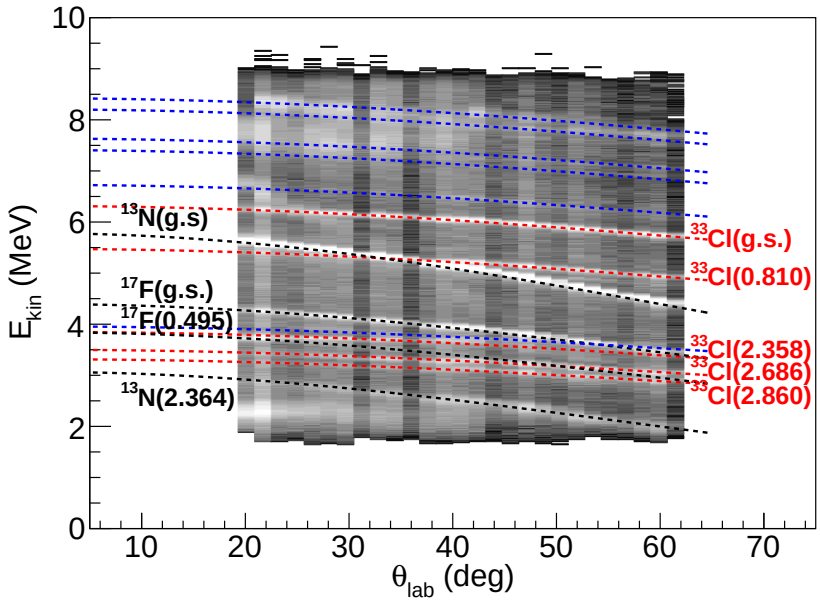

Figure 2. Deuteron kinematic lines E_{kin} vs θ_{lab} obtained in this experiment. The plot is built merging data from both telescope configurations used in the experiment. Blue and red dashed lines show the calculated kinematic lines respectively for contaminant reactions and ^{32}S(^{3}He,d)^{33}Cl reactions. ^{12}C and ^{16}O contaminants in the target are responsible for ^{13}N and ^{17}F residual nuclei lines, respectively.

^{33}Cl nucleus, indicated by labels. Black dashed lines are concurrent (^{3}He,d) reactions occurring on ^{12}C and ^{16}O contaminants present in the target backing. The latter lead, respectively, to ^{13}N and ^{17}F residual nuclei. We observe an overall good agremment of calculated and experimental lines, indicating the good geometrical consistency of the apparatus and the good quality of the energy calibration. In all the angular regions where the lines do not significantly overlap, we can extract the yield of the ^{32}S(^{3}He,d)^{33}Cl reactions, unambiguously.

The angular range shown in Figure 2 is segmented into angular regions according to the recorded statistics and to minimize the θ overlap between pseudo-telescopes of contiguous regions. We obtain over 30 separated angular regions. In each region, we extract the yield of all the observed ^{32}S(^{3}He,d)^{33}Cl reactions using a multi-gaussian fit of the data. Fig. 3 shows an example of such fitting procedures, for a pseudo-telescope located at $\theta_{lab} \approx 43.7°$. The multi-fit procedures accounts also for contaminant peaks due to other elements in the target. Interestingly, we are able, for the first time, to extract the yield of the ^{32}S(^{3}He,d)^{33}Cl reaction leading to the 2.358 MeV state in ^{33}Cl, which is close to the proton emission threshold and is the only excited state that sizeably contributes to the ^{32}S(p,γ)^{33}Cl reaction in stellar environment.

The differential cross section in absolute units is obtained via an internal normalization that exploits the Rutherford scattering of ^{3}He on Zn, with the procedure detailed in Ref. [43]. Fig. 4 shows the experimental differential cross section angular distributions for all the ^{33}Cl states clearly seen in Fig. 3. Absolute cross section data was interpreted by comparing them with

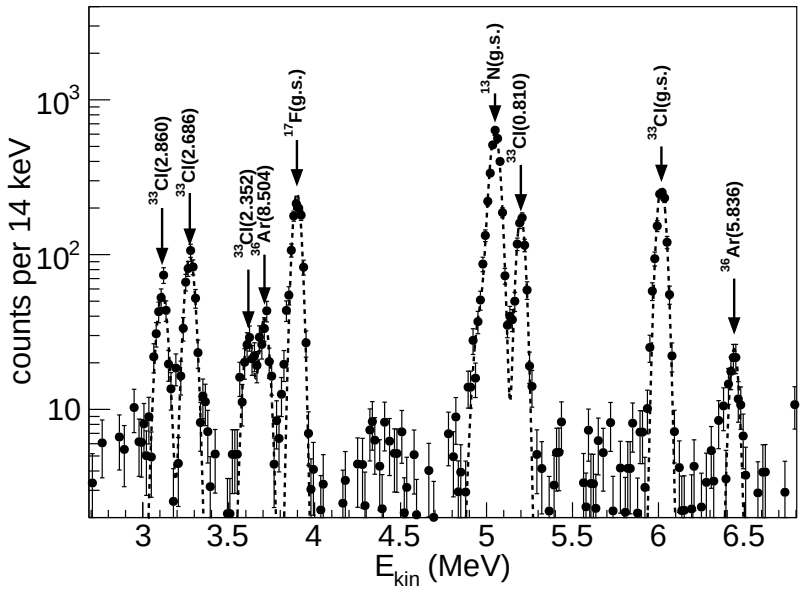

Figure 3. Deuteron energy spectrum obtained at $\theta_{lab} \approx 43.7°$ fitted with multiple Gaussian functions. Results of the simultaneous fit are shown with the dashed line. Peaks associated with well-identified exit channels are labeled.

finite-range DWBA and Coupled Reaction Channels (CRC) calculations (respectively, red lines and blue dashed-lines in Fig. 4. In our DWBA and CRC calculations, we considered one-proton transfer to the $1d_{3/2}$, $2s_{1/2}$, $2p_{3/2}$ and $1f_{7/2}$ orbitals. Further details of the assumptions and parameters used for the theoretical calculations can be found in Ref. [43].

We obtain a completely satisfactory fit of data for the g.s., the 2.685 MeV, and the 2.846 MeV states of ^{33}Cl. For the 0.810 MeV state, we observe a good agreement between experiment and calculations at larger angles, while data at angles smaller than 40° show experimental cross sections larger than the both calculations. This trend was seen also in the [41, 40] data, possibly indicating some inadequacy of the theoretical models in the description of the reaction mechanism. For the astrophysically important state (2.352 MeV), we obtain an overall good reproduction of the absolute scale of the cross section, but we are not able to finely reproduce the trend of data. This could be caused, even if unlikely, by nuclear reactions on contaminants that pollute the small peak associated with this transition and seen in the ejectile spectrum. Another possible explanation could be related to the nature itself of this transition, which might be affected by a non-direct components.

Table 1 summarizes the spectroscopy of low-lying ^{33}Cl states obtained in the present analysis, compared to the prescriptions of the literature. The C^2S_p value obtained via χ^2 minimization for the g.s. of ^{33}Cl is $C^2S_p = 0.73$. This value is in excellent agreement with the one of Ref. [40] at 29.7 MeV (0.70). We observe deviations up to about 25% with the values recommended in Refs. [41, 44]. The population of the 0.81 MeV excited state is attributed to the proton transfer in the $2s_{1/2}$ orbital. For this state, we obtain $C^2S_p = 0.25$, which is very close to those suggested in Refs. [45, 41, 44]. For the 2.352 MeV state, the only published data leading to an estimate of C^2S_p are the 34.5 MeV data of Ref. [40]. For this state, we obtain the best fit of data assuming $\ell = 2$ and $J^\pi = 3/2$. This leads to $C^2S_p = 0.73$, which is in qualitative agreement with the

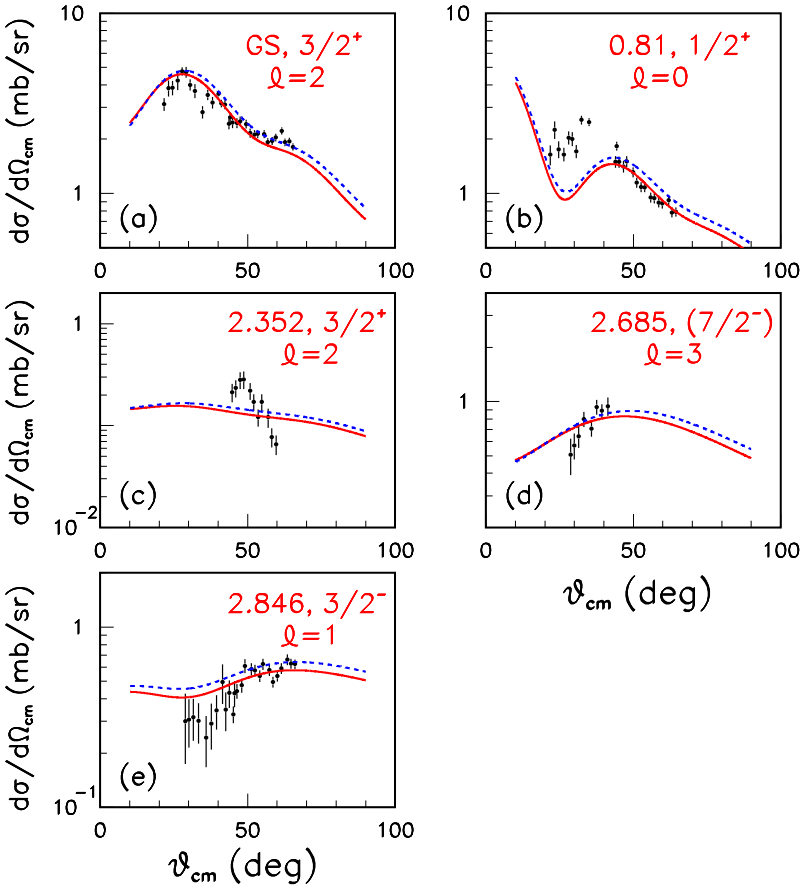

Figure 4. Differential cross section angular distributions for the ^{32}S(^{3}He,d)^{33}Cl reactions leading to the 0 (a), 0.81 (b), 2.352 (c), 2.685 (d), and 2.846 (e) MeV states in 33Cl. Red solid lines are the results of the CRC calculations; blue dashed lines show the results of the DWBA calculations.

estimate of Ref. [40] (0.061). Concerning the 2.685 MeV state, the literature reports contrasting J^{π} assignments [39]. Most of previously published data [41, 40, 44, 46] tend to support the one-proton transfer to the $1f_{7/2}$ shell. In the present work, we obtain an improved χ^2 by considering $\ell = 3$ and a $J = 7/2^{-}$ assignment. The $C^2S_p = 0.44$ obtained from our CRC calculations is close to the findings of Refs. [45, 41, 40]. Finally, for the transition to the 2.846 MeV state in ^{33}Cl, we determine a $C^2S_p = 0.28$ value, which is smaller than those suggested in the literature at similar energy [41]. This difference can be attributed to the smaller values of cross section reported in this work.

4. Conclusions and Perspectives

In this work, we investigated the ^{32}S(^{3}He,d)^{33}Cl one-proton transfer reaction, at 9.68 MeV, using the new hodoscope of silicon detectors OSCAR. The high angular segmentation of the detector and the excellent energy resolution allowed to extract the yield of the transitions to the g.s., and to the 0.810 MeV, 2.352 MeV, 2.685 MeV, 2.846 MeV excited states in ^{33}Cl, unambiguously. The angular distributions of the differential cross section, in absolute units, are obtained via an

Table 1. Spectroscopy of low-lying states in ^{33}Cl obtained in this work. The last column shows the C^2S values obtained in our analysis. Values from Refs. [45, 44, 40, 41, 47] are also shown. For Ref. [40], the authors report data for 2 different bombarding energies, namely 29.7 MeV (a) and 34.5 MeV (b).

^{33}Cl E_x (MeV)	J^π	ℓ	[45]	[44]	[40] (a)	[40] (b)	[41]	[47]	This Work
0	$3/2^+$	2	0.47	0.90	0.70	0.63	0.54	0.86	0.73
0.81	$1/2^+$	0	0.22	0.29	0.32	0.37	0.22	0.37	0.25
2.352	$3/2^+$	2	-	-	-	0.061	-	-	0.073
2.685	$(7/2^-)$	3	0.52	0.73	0.50	0.41	0.52	-	0.44
2.846	$3/2^-$	1	0.47	0.55	0.50	0.58	0.72	-	0.28

internal normalization procedure that exploits Rutherford scattering on Zn. For the first time, we report data free from contaminants for the 2.352 MeV state.

We perform detailed finite-range DWBA and CRC calculations to interpret the cross section values measured in this work. One-proton spectroscopic factors are extracted for all the observed transitions. The C^2S_p values obtained in this work are compared with the findings of previous investigations and theoretical models capable to describe the structure of *sd*-shell nuclei. The one-proton spectroscopic factor obtained for the 2.352 MeV state is in reasonable agreement with the only previous estimate reported in the literature, but with a lower level of background. This result can help to refine the ^{32}S(p, γ)^{33}Cl reaction rate at low temperatures $T < 0.1$ GK, which is relevant for astrophysics.

References

[1] Lombardo I *et al.* 2014 *Bulletin of the Russian Academy of Sciences: Physics* **78** 1093
[2] Lombardo I *et al.* 2014 *J. Phys. Conf. Ser.* **569** 012068
[3] Lombardo I *et al.* 2016 *J. Phys. G.* **43** 45109
[4] Gade A *et al.* 2008 *Phys. Rev. C* **77** 044306
[5] Charity R *et al.* 2020 *Phys. Rev. C* **102** 044614
[6] Wylie J *et al.* 2021 *Phys. Rev. C* **104** L061301
[7] Jin Y *et al.* 2021 *Phys. Rev. Lett.* **127** 262502
[8] Bishop J *et al.* 2019 *Phys. Rev. C* **100** 034320
[9] Dell'Aquila D *et al.* 2017 *Phys. Rev. Lett.* **119** 132501
[10] Lombardo I *et al.* 2018 *Phys. Rev. C* **97** 034320
[11] Risitano F *et al.* 2022 *Nuov. Cim. C* **45** 60
[12] He J J *et al.* 2018 *Chin. Phys. C* **42** 15001
[13] Spitaleri C *et al.* 2020 *Eur. Phys. J. A* **56** 18
[14] Lombardo I *et al.* 2019 *Phys. Rev. C* **100** 044307
[15] Piantelli S *et al.* 2017 *Phys. Rev. C* **96** 034622
[16] Borderie B *et al.* 2018 *Physics Letters B* **782** 291–296
[17] DeFilippo E *et al.* 2009 *Acta. Phys. Pol. B* **40** 1199
[18] Bougault R *et al.* 2018 *Phys. Rev. C* **97** 024612
[19] Morelli L *et al.* 2016 *J. Phys. G: Nucl. Part. Phys.* **43** 045110
[20] Cicerchia M *et al.* 2021 *J. Phys. G. Nucl. Part. Phys.* **48** 045101
[21] Russotto P *et al.* 2015 *Phys. Rev. C* **91** 014610
[22] Lombardo I *et al.* 2010 *Nucl. Phys. A* **834** 458c
[23] Zhu K *et al.* 2020 *Nucl. Instr. Meth. Phys. Res. A* **967** 163826
[24] Acosta L *et al.* 2016 *J. Phys. Conf. Ser.* **730** 012001
[25] Dell'Aquila D *et al.* 2017 *J. Phys.: Conf. Ser.* **876** 012006
[26] Dell'Aquila D *et al.* 2019 *Nucl. Instr. Meth. Phys. Res. A* **929** 162
[27] Cardella G *et al.* 2015 *Nucl. Instr. Meth. Phys. Res. A* **799** 64
[28] Martorana N *et al.* 2018 *Phys. Lett. B* **782** 112

[29] Dell'Aquila D *et al.* 2016 *EPJ Web of Conf.* **117** 06011
[30] Dell'Aquila D *et al.* 2016 *Nuov. Cim. C* **39** 272
[31] Valdré S *et al.* 2019 *Nucl. Instr. Meth. Phys. Res. A* **930** 27
[32] Pastore G *et al.* 2017 *Nucl. Instr. Meth. Phys. Res. A* **860** 42
[33] Cappuzzello F *et al.* 2016 *Eur. Phys. J. A* **52** 167
[34] Fernández-Domínguez B *et al.* 2011 *Phys. Rev. C* **84** 011301
[35] Nevelinga R *et al.* 2011 *Nucl. Instr. Meth. Phys. Res. A* **654** 29
[36] Dell'Aquila D *et al.* 2018 *Nucl. Instr. Meth. Phys. Res. A* **877** 227
[37] Wildenthal B *et al.* 1971 *Phys. Rev. C* **4** 1708
[38] Castel B *et al.* 1971 *Nucl. Phys. A* **162** 273
[39] Chen J and Sing B 2011 *Nucl. Data Sheets* **112** 1393
[40] Kozub R and Youngblood D 1972 *Phys. Rev. C* **5** 413
[41] Inglima G *et al.* 1975 *Nuov. Cim. A* **26** 211
[42] Iliadis C *et al.* 2001 *Astr. J. Suppl. Ser.* **134** 151
[43] Lombardo I *et al.* 2021 *J. Phys. G Nucl. Part. Phys.* **48** 065101
[44] Morrison R 1970 *Nucl. Phys. A* **140** 97
[45] Graue A 1966 *Phys. Nor.* **2** 7
[46] Moss C 1970 *Nucl. Phys. A* **145** 423
[47] Vernotte J *et al.* 1994 *Nucl. Phys. A* **571** 1